



Science Arts & Métiers (SAM)

is an open access repository that collects the work of Arts et Métiers Institute of Technology researchers and makes it freely available over the web where possible.

This is an author-deposited version published in: <https://sam.ensam.eu>
Handle ID: <http://hdl.handle.net/10985/23031>

To cite this version :

Rabii CHEKKOUR, Adil BENAARBIA, George CHATZIGEORGIOU, Fodil MERAGHNI, Gilles ROBERT - Effect of thermo-hygro glycol aging on the damage mechanisms of short glass-fiber reinforced polyamide 66 - Composites Part A: Applied Science and Manufacturing p.107358 - 2022

Any correspondence concerning this service should be sent to the repository

Administrator : scienceouverte@ensam.eu



Effect of thermo-hygro glycol aging on the damage mechanisms of short glass-fiber reinforced polyamide 66

Rabii CHEKKOUR^a, Adil BENAARBIA^a, George CHATZIGEORGIOU^a, Fodil MERAGHNI^{a*}, Gilles ROBERT^b

^aArts et Métiers Institute of Technology, CNRS, Université de Lorraine, LEM3 UMR CNRS 7239, F-57070 Metz, France.,

rabii.chekkour@ensam.eu, adil.benaarbia@ensam.eu, georges.chatzigeorgiou@ensam.eu, fodil.meraghni@ensam.eu

^bDOMO Chemicals – Polytechnyl SAS, Usine de Belle Etoile, 69190 Saint-Fons, France,
gilles.robert@domo.org

Abstract

This paper aims at studying the effect of ethylene glycol aging on the overall behavior and the damage mechanisms of the Polyamide 66 (PA66) and the short glass fiber reinforced polyamide 66 (PA66/GF). To this end, a proper experimental aging setup is designed and presented for conditioning the samples in glycol at different aging durations. The glycol absorption effect is analyzed through the swelling and the mass variation (uptake). Moreover, monotonic tensile tests are performed to study the glycol aging effect on the PA66 and PA66/GF. SEM (Scanning Electron Microscopy) investigation is then performed to characterize the damage mechanisms and their evolution with the increase of the aging duration. X-ray micro-computed tomography (μ CT) observations are also carried out to quantify the damage depending on the aging duration, the material, and the area of interest (AOI). Experimental findings show that the glycol absorption is more important for the PA66 unreinforced matrix than for the short glass fiber reinforced PA66 composite. In addition, the stiffness, as well as the material deformability, are found to be significantly affected by the glycol aging. In terms of composite degradation, the main damage mechanisms are the damage at fiber's end and the fiber-matrix interface, and for the high aging durations, cavitation in the polymer matrix is observed. The X-ray μ CT investigation has indicated pronounced damage mostly located at the core and surface of the samples, which is due to the well-known shell-core microstructure of injected PA66/GF composites. All these conclusions lead to infer the significant and irreversible effect of glycol aging on the bulk mechanical behavior and damage mechanisms of the investigated materials.

Keywords

Short glass-fiber reinforced PA66, Glycol aging, Damage mechanisms, SEM, X-ray microtomography.

1. Introduction:

In the automotive industry, glass fiber reinforced polyamides (PA/GF) are employed in several in-service components (e.g., oil circuit, cooling system). During their real service conditions, cooling circuit components exposed to thermo-chemo-mechanical coupling can exhibit early breakage due to the presence of coolant liquid (a water-ethylene glycol equi-volume mixture) in addition to fatigue, which significantly affects the thermomechanical properties, leading to their progressive degradation [1]–[5]. The effect of humidity and related durability on the material have already been investigated in the literature. However, the interactions between the material and coolant, occurring at different scales, have not been completely addressed in the open literature, and require deeper qualitative and quantitative investigations. These interactions are of high interest when dealing with damage mechanisms prior to the macroscopic failure. A thorough study on the effect of the thermo-hygro-glycol aging will contribute to improving the durability of the thermoplastic composite material and the related components employed for automotive applications. It will also avoid the oversizing of the composite components, notably that are in contact with coolant liquid.

In the open literature, many experimental works have been conducted in the past in order to study the composite behavior within varied aging media [6], [7]. For instance, Ledieu [6] has performed an experimental investigation to deal with the aging mechanisms of PA66/GF material exposed to several aging media (e.g., water, glycol, coolant) at different temperatures and varied aging durations. The objective was to explore the link between the material mechanical properties and the associated changes in the macromolecular chemical structure (e.g., molar mass, degree of crystallinity, etc.). The author performed classical gravimetric analysis on aged samples in glycol at 120 °C, 130 °C, and 140 °C, in coolant at 90 °C, 100 °C, and 108 °C, and in water at 100 °C. In this work, it has been concluded that the high aging temperatures promote the increase of the sorption of both glycol and coolant by the PA66. Alternatively, numerous studies have been conducted to investigate the water aging effect on polyamide materials and the associated composite [1]–[4], [8], [9]. Benaarbia [10] has noticed that the material thermomechanical behavior and the associated energy responses significantly changed when changing the relative humidity. Arif [8], [11] investigated the water aging effect on the quasi-static and fatigue mechanical responses of PA66/GF material subjected to bending and tensile tests at different relative humidity conditions. Using in-situ SEM tests, the authors identified mechanisms for damage initiation and accumulation. All the aforementioned studies mainly focused on the physical interactions between the water content and the material thermomechanical features.

Limited studies have been reported in the open literature that investigate the aging effect of the ethylene glycol on PA66/GF. Pires [7] carried out monotonic tensile tests on PA66 samples aged in glycol at different aging durations. The author noticed that the ultimate tensile stress decreased with increasing aging duration. However, the ultimate strain increased till a certain aging duration, then decreased for longer aging durations. This has been explained by the fact that the glycol molecule causes a modification of the polyamide molecular chains, bringing about a *plasticization* phenomenon and a glass transition decrease followed by an embrittlement of the material, which has been observed for large aging durations. This observation has been confirmed by Ledieu in [6]. Besides that, the plasticization also affects the glass transition temperature that goes from 91 °C in the initial state to – 4 °C after the glycol aging. Ledieu concluded that the plasticization phenomenon is more significant for the glycol absorption than for the water. The chemical interaction between the glycol and the material has not been noticed at the studied aging temperatures; no glycolysis has been observed at 130 °C, suggesting that the irreversible damage is mainly induced by the physical interaction.

Regarding the damage mechanisms, numerous damage investigations have been conducted in the literature on polymer matrix based composites using different destructive and non-destructive techniques such as SEM, X-Ray microtomography, acoustic spectroscopy, etc. [11]–[15]. An initiation and accumulation of damage scenario has been suggested by Sato et al. [16] for PA66/GF through SEM observations during monotonic tensile loading and confirmed by Arif et al. [11], with regard to relative humidity effects. Horst and Spoormaker [17], [18] observed similar damage mechanisms during fatigue tests, while Arif et al. [8] noticed that the fiber/matrix debonding is the most predominant damage mechanism. In a related note [11], the authors performed SEM investigations to study the effect of water uptake at different relative humidity conditions (dry-as-molded, RH50 and RH100) during in-situ bending tests conducted on PA66/GF samples. They observed that the increase of the relative humidity results in an early and more important damage, notably in the matrix phase. At 95 % of the ultimate stress, they noticed a fiber breakage and matrix cracks for the dry-as-molded samples. At 98 % of the ultimate stress, they observed matrix microcracks for the RH50 samples, and matrix microcracks as well as matrix deformation bands for the RH100 samples. Rolland et al. [12], [19] carried out tensile in-situ tests on PA66/GF at different relative humidity conditions. However, the effect of the glycol aging on damage mechanisms for PA66 and PA66/GF samples remains partially unexplored, especially in terms of damage initiation and accumulation in the open literature.

The novelty of this work is the experimental multiscale investigation of the glycol aging effect on the damage mechanisms of PA66/GF. This research constitutes an important first step to study the material behavior under thermo-hygro-glycol aging, by highlighting and understanding the aging influence of each coolant constituent before studying their combined effect. In this paper, we aim to emphasize the impacts of glycol aging on mechanical responses of PA66 and PA66/GF, and more precisely, on the damage mechanisms. A comparison between the humidity and glycol aging effects on the damage mechanisms for PA66/GF is presented. This study mainly focuses on the physical interaction between the glycol and PA66. The new contributions of the present work include: (i) An evaluation of the material degradation undergoing glycol aging to prevent early failure and allow proper improvement of the material durability. (ii) The glycol aging effect in terms of cross-section and mass variation of unreinforced PA66 and PA66/GF composites. (iii) The identification of damage mechanisms for glycol aged PA66/GF composite through SEM observations with respect to the aging duration. (iv) The damage quantification in terms of defects content through X-ray μ CT investigation on PA66 matrix and PA66/GF composites with different material configurations and aging durations.

The present paper is organized as follows: in Section 2, a brief description of the PA66/GF specimen preparation is followed by the short presentation of the aging procedure in glycol medium. In section 3, the experimental results from monotonic tensile tests are presented, followed by a damage mechanisms investigation performed in two steps; first, post-mortem observations using SEM to identify and to emphasize the dominant damage mechanisms, and then void analyses through X-ray μ CT to quantify the void content and its evolution. Finally, in Section 4, concluding remarks are presented and some prospects are suggested for further work.

2. Material description and experimental procedure

2.1 Material description

The materials investigated in the experiments are: (i) unreinforced PA66 and (ii) short E-glass fiber reinforced PA66 provided by DOMO Chemicals in the form of injection-molded rectangular plates (360mm-in-length, 100mm-in-width and 3mm-in-thickness), and commercially available under the trade name of A218V30 BK 34NG. It is worth mentioning that in this work, the provided specimens from DOMO Chemicals have black pigment. The injection process parameters are identical to those reported by Arif [20], Klimkeit [21], and Rolland [22]. For the sake of completeness, they are recalled as follows: mold temperature 85 °C; injection pressure 927 bars; injection speed 42 cm³/s; and the screw rotation speed 150 rpm. It is worth mentioning that the reference A218 BK 34NG represents the PA66 matrix whereas V30 stands for the reinforcement weight content of 30 %,

which corresponds to 16.5 % of fiber volume content as mentioned in [12], [20] and [23]. The average nominal fiber length in the manufactured composite is 250 μm whereas the average nominal fiber diameter is 10 μm . Both average values have been confirmed through X-ray microtomography by H. Rolland [12]. The glass fibers have been subjected to sizing treatment. The latter is specific for the polyamide matrices. It improves the fiber/matrix interfaces and ensures a slow deterioration during the injection manufacturing process.

Typical plates show complex Fiber Orientation Distributions (FOD) induced by the mold-flow direction (MFD), that has been measured by DOMO Chemicals using X-ray microtomography and reported in Chen et al. [23]. The typical microstructure distribution exhibits the well-known shell-core structure [8], [11], [23] where three layers can be observed as presented in Figure 1. In this figure, the mCT observed region was extracted from the central part (gage part) of the specimen in as-received configuration. The shell layer is characterized by a fiber orientation similar to the mold flow direction, representing around 90 % of the sample's thickness [8], while the fibers in the core layer are oriented transversally to the mold flow direction, representing 5 % of the sample's thickness. In addition, the remaining 5 % form a thin layer at the surface with random fiber orientation, due to the contact between the mold wall and the melted polymer. This particular microstructure with three layers composition is commonly observed in injection molded short fiber composites. It engenders a microstructure driven thermomechanical response [23] and undeniably affects the damage mechanisms initiation and accumulation.

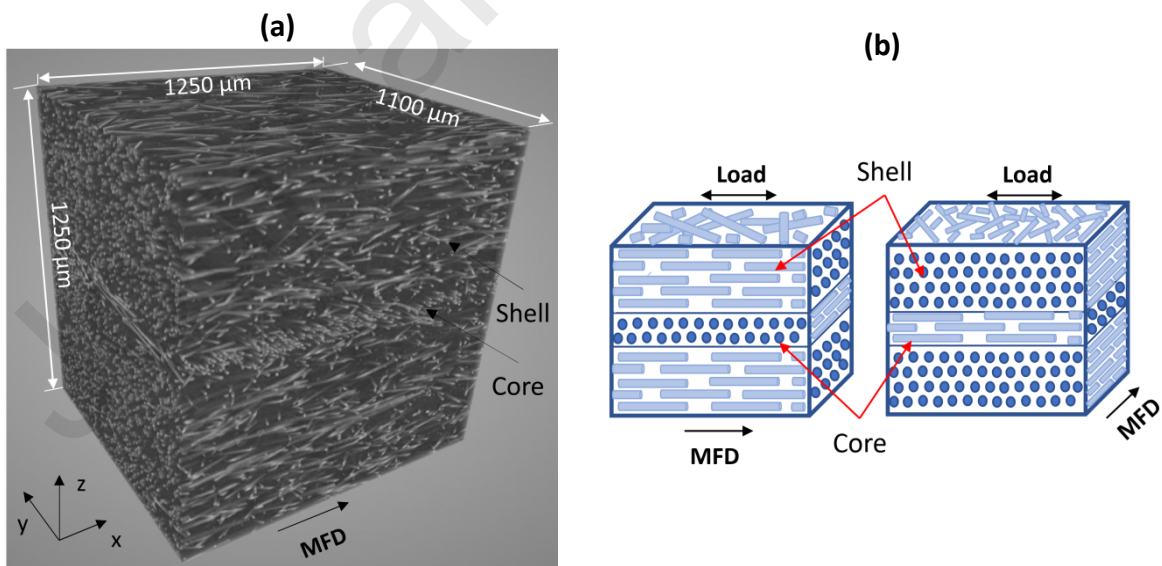


Figure 1. (a) Typical reconstructed volume for injected reinforced polyamide with transversally-oriented fibers using X-Ray microtomography with voxel size of 0.55 μm , in which the shell-core microstructure is clearly observed. (b) Schematic diagram highlighting the fiber orientation in the shell-core microstructure with regard to the loading direction.

2.2 Sample preparation and aging conditions

Prior to the experiments, PA66/GF samples are obtained using water jet hyperbar machining process. They are machined in three orientation directions with respect to the mold-flow direction, namely 0° , 45° , and 90° . The samples are 96 mm in overall length, with 14 mm in gage width and 3 mm in thickness as illustrated in Figure 2. The geometry of the specimen has been optimized through finite element calculations to avoid stress concentrations between the gage part and the clamping part.

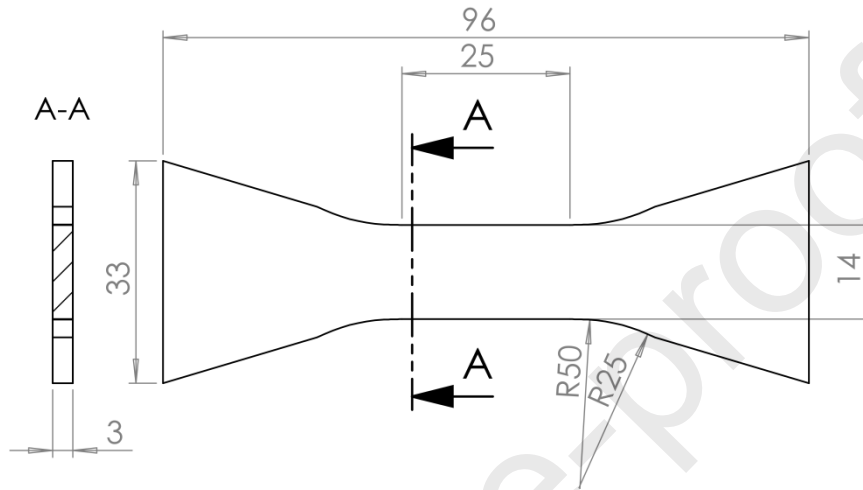


Figure 2. Dog bone samples with dimensions in mm, obtained by water-jet hyper bar machining. The thickness is set at 3 mm.

To ensure the presence of the glycol aging only without any water interference, the samples have undergone a pre-conditioning procedure in order to achieve a dry-as-molded state. The samples are placed in a conditioning chamber at temperature of 80°C under a dry environment within a vacuum for at least 16 hours as preconized by the industrial partner DOMO Chemicals.

To replicate the real in-service conditions effect on the material that usually take years, an accelerated aging approach [24] has been adopted for this study. The material usually undergoes specific conditions in terms of temperature, pressure, humidity, etc., and since glass fiber reinforced polymers behavior is strongly dependent on time and temperature [4], higher aging temperature has been selected in order to shorten the aging time. To that end, an original inhouse experimental aging setup has been designed and fabricated to achieve samples aging in glycol medium at different aging durations. The device scheme presented in Figure 3 displays the main components of the instrumented experimental platform. These include a high-pressure tank, a heating collar with a platinum sensor (PT100), providing accurate temperature measurements in the tank under pressure, and finally the thermal regulation box for temperature control. A sample holder has been designed in order to maintain the samples floating in the aging medium with a capacity of 36 samples per aging. A magnetic stirrer (agitator) is employed to

ensure a homogenous medium temperature. A pressure valve with a manometer is added to keep the pressure under control inside the tank and to ensure that it will not exceed a preset pressure level of 7 bars. Rock wool is used around the tank for thermal insulation. The setup is surrounded by metallic and plexiglass protection to ensure the safety of the user. The device is connected to pressurized air on the outside to reduce the cooling time.

A rigorous experimental protocol has been established to ensure proper operation, repeatability, and compliance with safety and environmental commitments.

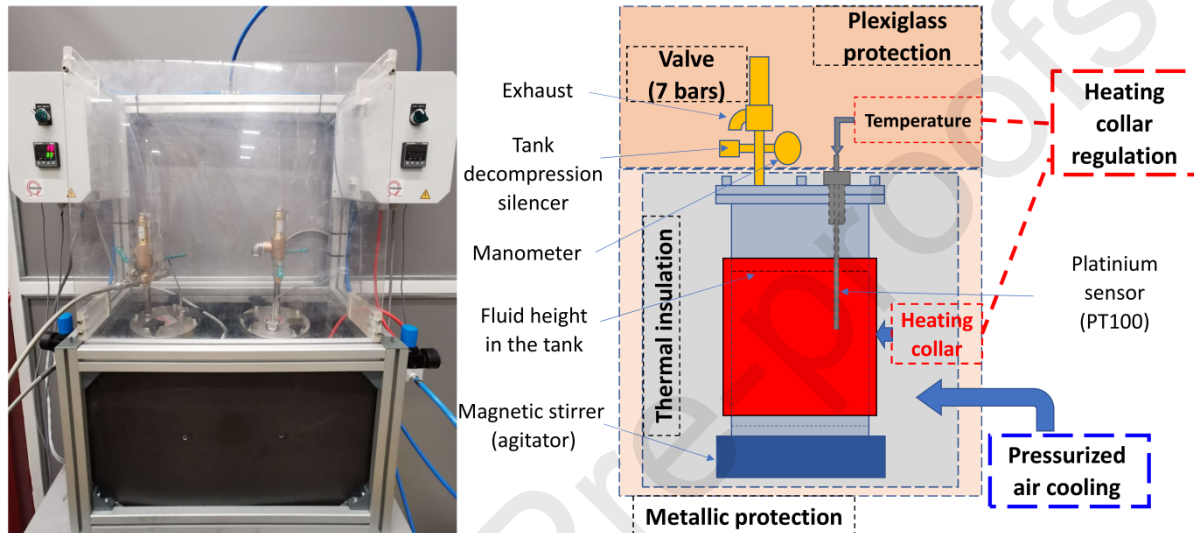


Figure 3. Overview of the developed aging device: scheme and components used for the aging of PA66 and PA66/GF samples.

In order to thoroughly study the glycol aging effect on the PA66 and PA66/GF materials, several aging durations have been selected, namely: 1, 2, 5, 10, 12 and 20 days at an aging temperature of 130 °C. The determination of the aging durations has been chosen accordingly to the automotive industry standards, such as Valeo NVB 15009 – Class 3 and DBL 5406-2021. The requirement is to produce similar aging effects with in-service real-life conditions of a composite component by accelerated procedures that last 500 hours, which correspond approximately to 20 days. The intermediate aging durations allow to monitor the evolution of the material's behavior. A volume ratio of 15 between the PA66 and the aging medium (glycol) has been set to ensure the same aging conditions for all the aging durations, to conserve a dilute aging solution with a constant pH level. The samples' cross-section dimensions at the gage area as well as the weight have been measured before and after the aging to monitor the swelling effect.

3. Mechanical testing and microstructure observations

The mechanical characterization has been performed by conducting monotonic tensile tests on PA66 and PA66/GF dog bone samples. A Zwick/Roell Z050 testing machine with a load cell capacity of 50 kN has been employed for the experiments, coupled with an Epsilon axial extensometer with a gage length of 25 mm, as shown in Figure 4. A sample setting tool has been designed and fabricated using 3D printing to ensure the sample alignment with the loading axis and to avoid any induced twisting moment. The tests have been strain controlled and carried-out at a nominal strain rate calculated from the displacement of the crosshead with a value of $\dot{\epsilon} = 2 \cdot 10^{-3} \text{ s}^{-1}$ at room temperature.

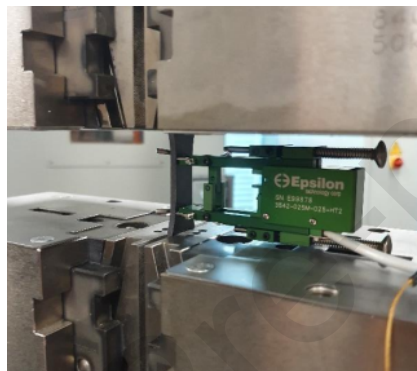


Figure 4. Image of the tensile test setup on the Zwick/Roell Z050 machine displaying the mounted sample and the extensometer.

Once a sample reached the macroscopic failure induced by the monotonic tensile load, it is then prepared for the SEM post-mortem observations of the damage mechanisms occurring close to the failure zone. To obtain a region with diffuse damage under tensile loading, the area of interest should be around the failure zone. This area of interest is far away from the loading introduction zone (clamping regions). SEM observations have been first conducted on 7 mm by 7 mm squares, cut at the rupture edge (see Figure 5) with a Secotom saw, in order to identify the nature of the damage mechanisms leading to the macroscopic failure. A thermosetting resin has been utilized to enhance the surface polishing (Figure 5). The polishing procedure started with 0.7 mm material removal to observe the skin layer. It was followed by three polishing steps using 9 μm and 3 μm abrasive papers as a first step, then using a cloth with 1 μm diamond paste. The surface has then undergone ultrasonic cleaning to get rid of the particles resulting from the polishing, followed by a chemical attack using a nitric acid solution at 2 % for 15 seconds. Finally, a thin layer of gold has been applied on the surface of the samples through metallization device (deposition).

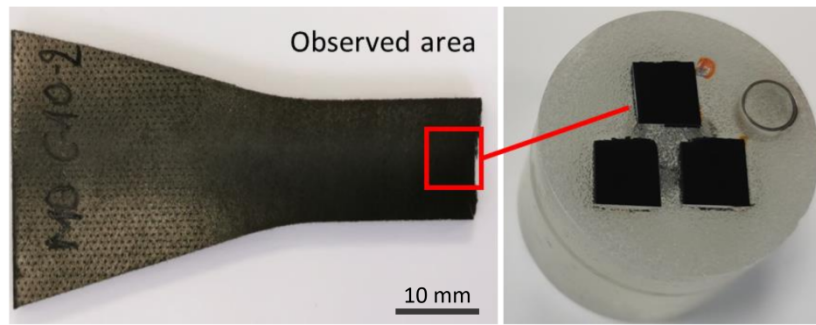


Figure 5. Observed area for SEM investigation chosen close to the failure zone of the sample.

X-ray microtomography acquisitions have been also performed on the ruptured samples after monotonic tensile loading for a 3D qualitative and quantitative analysis of the damage that the material undergoes. The X-ray micro-computed tomography has been performed at the LEM3 facilities (Metz, France). The acquisition area is a cylinder with a diameter of 4.5 mm and a height of 4.2 mm, and is also located next to the fracture area where the damage is mostly localized. The voxel size used for the acquisition is 2.04 μm . The X-ray beam parameters are: tube power 6.9 W, tube voltage 65 kV, tube current 106 μA . The imager (flat panel) parameters are: resolution 2320 x 2336 pixels, frame acquisition rate (FPS) 0.50 / s, number of average frames 6.

4. Experimental results and discussions

4.1. Mass and cross-section variations of aged samples

The samples glycol absorption has been investigated through the measurement of the mass uptake and the cross-section variation before and after the aging for each aging duration. The mass measurements have been performed using a device with a resolution of 0.1 mg. After the aging procedure, the overload of glycol on the surface of the samples is wiped off using absorbent paper to avoid disturbing the mass measurements. The cross-section variation has been analyzed by measuring the width and the thickness evolution at the gage area for two samples before and after aging.

The mass variation is displayed in Figure 6 for PA66 and PA66/GF samples in different fiber orientations for the selected aging durations. The mass variation is measured through classical gravimetry method and is presented in percentage as the mass difference before and after aging divided by the initial mass before aging. Overall, the results show an increase in the samples' mass variation for higher aging durations. One can notice that, the absorption of the glycol by the samples is significant after 1 day of aging. It gradually increases when increasing the aging durations. It is also noticed that the PA66 material is more sensitive to the glycol absorption compared to the reinforced composite, regardless of the fiber orientation, notably for the large aging durations.

However, for short aging durations (1 and 2 days) the aged composite shows a slightly higher weight uptake for transverse fiber-orientation (90°) samples compared to the case of 45° and longitudinal fiber-orientation samples (0°) with respect to the MFD.

After the glycol aging, a comparison between the surface states of unaged and aged PA66 samples is presented in Figure 7. In the unaged configuration (Figure 7.a) the sample's surface is smoother without any apparent damage or cracks. For the 12 days aged samples (Figure 7.b), the initiation of few cracks is observed. These cracks evolve by accumulation leading to a large crack network as it is noticed for the 20 days aged sample (Figure 7.c). This leads to infer that the material undergoes severe damage beyond the critical aging duration of 12 days. It also explains the sudden evolution of the mass variation for the samples aged for 12 and 20 days as illustrated in Figure 6, in which the cracks are filled with more glycol compared to the other aging durations that do not exhibit any crack on the surface. A swelling phenomenon induced by the glycol aging duration has also been observed in most of the aged samples.

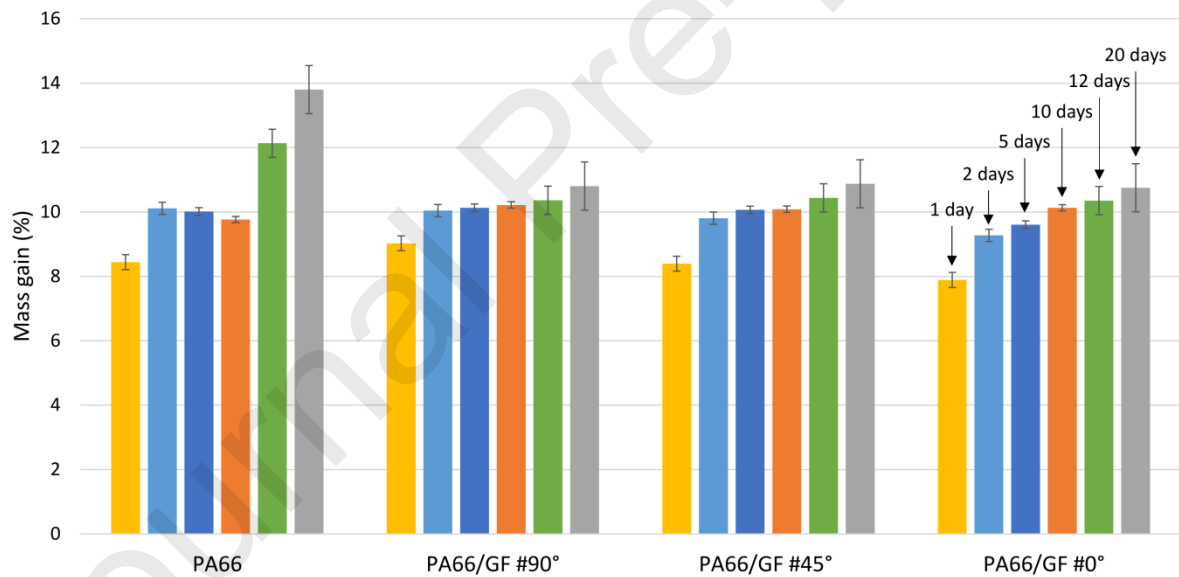


Figure 6. Mass variation of samples aged in ethylene glycol at different aging durations for both the unreinforced PA66 (matrix) and its short glass fiber reinforced composites. Comparison with the initial configurations before aging.

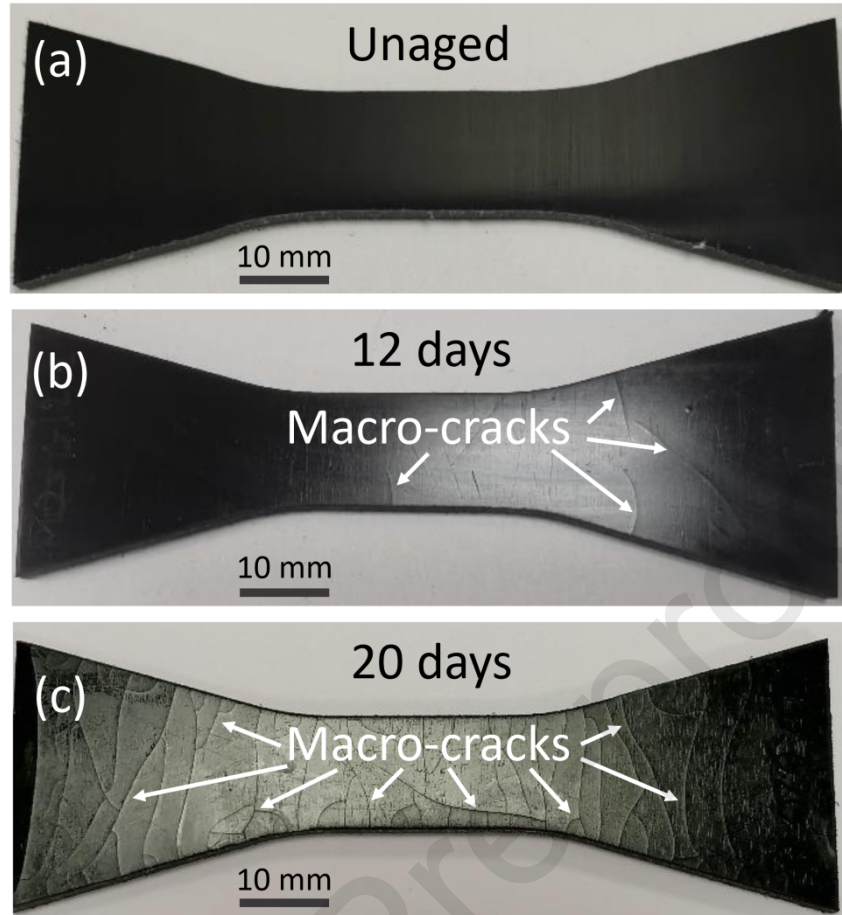


Figure 7. Overview of the surface state of PA66 samples after aging with respect to the case (a). Unaged. (b). Aged in glycol for 12 days. (c). Aged in glycol for 20 days. The results highlight the strong effect of glycol aging in which a macro-crack network appear on the surface of the aged samples.

In order to quantify the swelling phenomena in the gage part, the cross-section area has been measured before and after the glycol aging. This cross-section variation has been calculated by measuring the width and thickness of the samples in the gage part. It is presented in percentage as the cross-section difference before and after aging divided by the initial cross-section before aging. The cross-section variation is displayed in Figure 8 for PA66 and PA66/GF samples with different fiber orientations at different aging durations.

For reinforced composite samples, the cross-section is relatively increasing when the aging duration increases. However, a low increase in cross-section variation is observed for longitudinal fiber orientation samples (0°) compared to the other 45° and transverse fiber orientation (90°) samples. The differences between the considered fiber orientations can be attributed to the ability of the material to spitting-out the absorbed glycol. Indeed, it turns out that the material rejects more glycol when the fibers are oriented at 90° and 45° .

The polyamide (PA66) samples show a higher cross-section increase compared to the reinforced composite samples. This variation can be split into 3 different blocks with low (1-2 days), medium (5-10 days), and high (12-20 days) aging durations. In fact, it is noticed that for the PA66 the cross-sections increase considerably after 12 days of glycol aging.

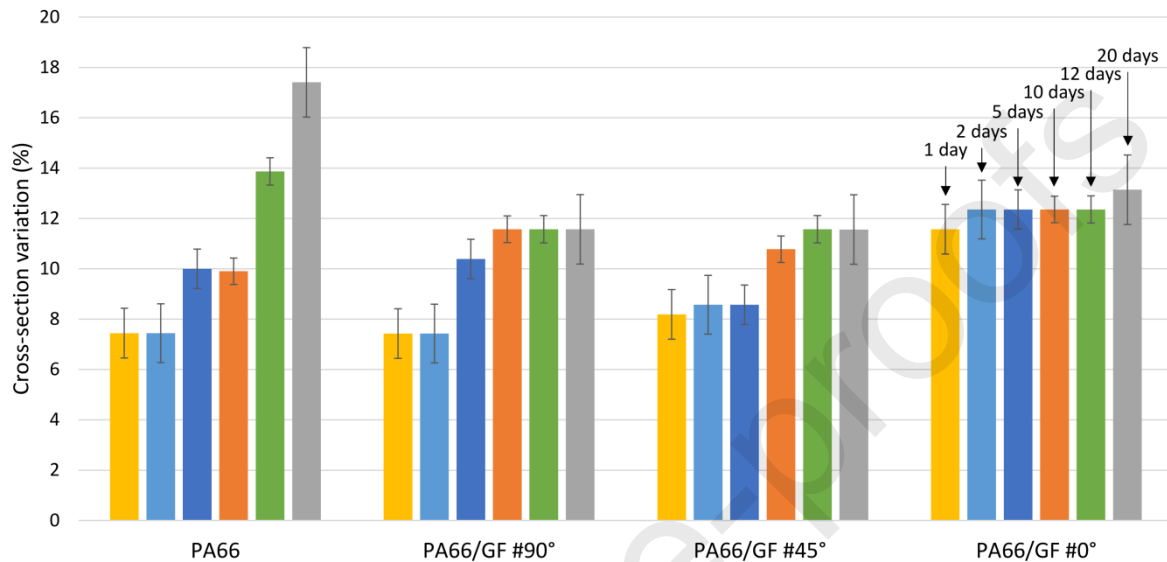


Figure 8. Cross-section variation of samples aged in ethylene glycol at different aging durations for both unreinforced PA66 and glass fiber reinforced PA66. Comparison with the initial sample state.

4.2. Monotonic tensile tests

Monotonic tensile tests have been performed on both unreinforced and reinforced composite samples after glycol aging at different aging durations. The corresponding overall tensile responses representing the evolution of the true stress versus the true strain curves are illustrated in Figure 9 with the unaged state being considered as a reference state. The mechanical response is demonstrated through normalized stress / normalized strain diagrams. This choice was dictated by the confidentiality requirements of the research consortium involving multiple stakeholders from industry and academia. In order to obtain more accurate mechanical responses, two samples have been tested for each aging duration. Overall, the mechanical responses have the same tendency for both tested specimens. Indeed, the discrepancy observed in terms of stress at failure for the two samples is less than 4 MPa, and it is less than 0.3 % for the strain at failure.

The overall behavior shows that for all aging configuration, the stiffness and stress at failure significantly decrease beyond 1 day of glycol aging. Nevertheless, the ductility and the strain at failure are fourfold higher than the unaged samples for an aging duration up to 2 days, then a decrease occurs when increasing the aging duration.

This behavior has been reported in several works among them [6], [7]. In these references, the authors explained this drastic reduction either by the plasticizing effect of the glycol or by a residual presence of humidity in the samples before the glycol aging mechanisms activation. Besides that, the tensile responses of PA66 samples aged at 12 and 20 days show significant stiffness reduction associated with a drastic drop of the ultimate strength. These aspects are due to the glycol aging effects amplified by the absence of glass fiber reinforcement. This observation fits exactly what has been inferred from the mass and cross-section variations results; the glycol absorption weakens the matrix as the mechanical properties of the material are drastically reduced.

For the composites, whatever the aging duration, the stress at failure is halved compared to the unaged state. However, the mechanical response for each case is different depending on the fiber orientation. For the longitudinally oriented fibers, the mechanical response is driven by the fibers, as they are in the same loading direction. The material displays a stiffer behavior with reduced ductility (low strain) compared to the other orientations. As for the 90° and 45° oriented fibers, the mechanical response is mainly driven by the PA66 matrix rheology, which is of 1st order importance. The effect of the fiber reinforcement is of 2nd order importance for these configurations. The material displays then lower stiffness with higher ductility leading to higher strain values compared to the 0° oriented fibers. Finally, for the unreinforced PA66 matrix aged for 12 and 20 days, macro-cracks have been observed on the sample surface (Figure 7) leading to early failure of the sample with drastic reduction in terms of stress and strain.

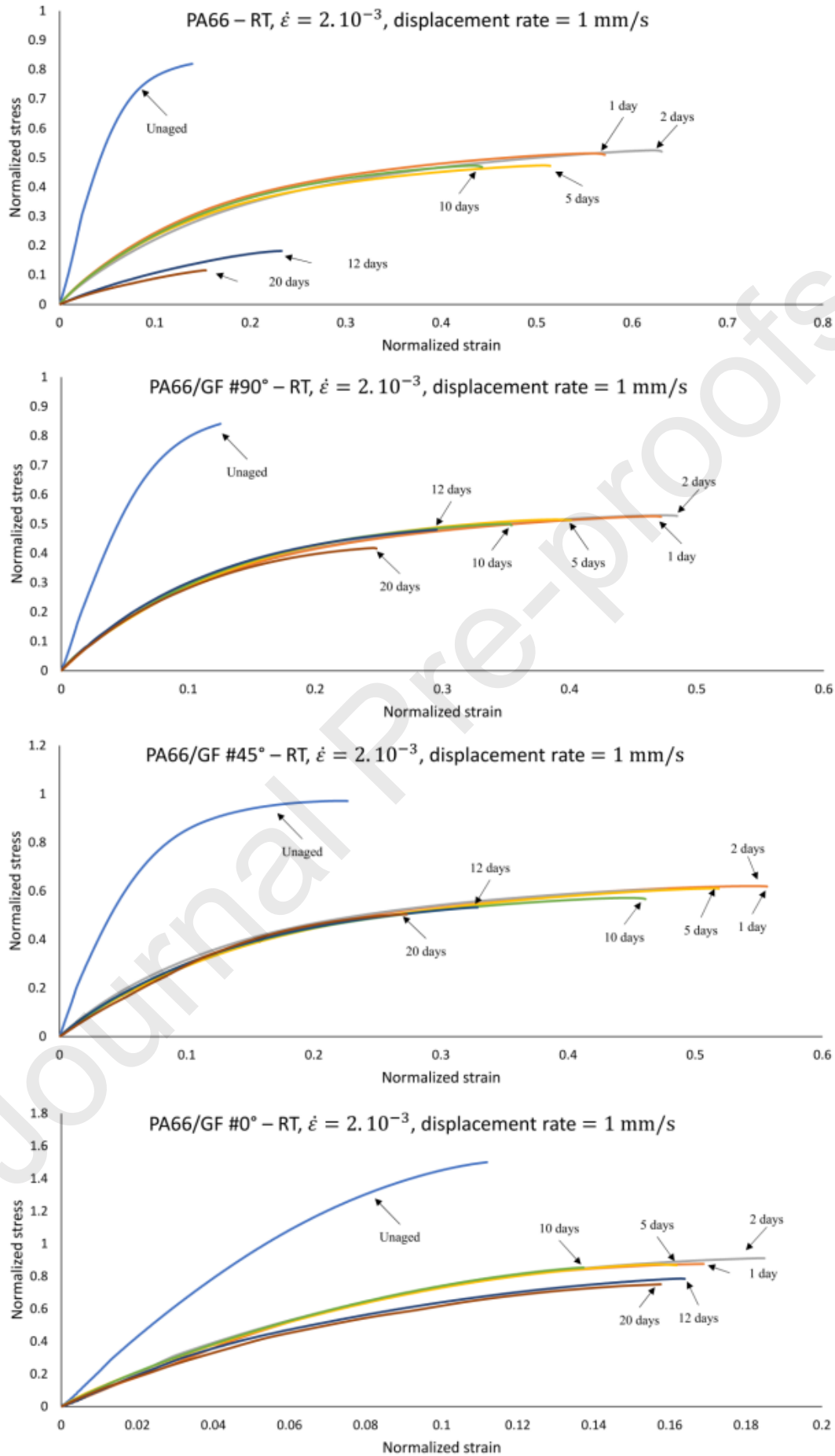


Figure 9. Normalized monotonic tensile test responses for glycol for unaged (dry) and aged samples at 1 day, 2 days, 5 days, 10 days, 12 days and 20 days. These tests have been performed at displacement rate of 1 mm/s, corresponding to a strain rate of $2 \cdot 10^{-3} \text{ s}^{-1}$. Noticeable stiffness reduction and stress at failure decrease with an increase in deformability and strain at failure up to 2 days followed by an embrittlement. This behavior suggests that different mechanisms are occurring during the aging process.

For a further study on the glycol aging effect on the mechanical behavior, stiffness degradation is plotted for PA66 matrix and glass fiber reinforced PA66 composites at different aging durations (Figure 10). The PA66 matrix displays a stiffness reduction of approximately 60% from 1 to 10 days of aging. For 12 and 20 days, a stronger degradation occurs in which 80% stiffness reduction is observed. Regarding the PA66/GF composites, and due to the fiber reinforcement, the stiffness evolution is not significantly affected by the aging duration for the composites with 45° and 90° oriented fibers. However, 70% stiffness loss represents an important degradation for all aging durations. For the longitudinally oriented fiber composites, and since the mechanical response is mainly driven by the fibers, the degradation is inferior to the other fiber orientations, but still displays a slight decrease with the increase of aging duration.

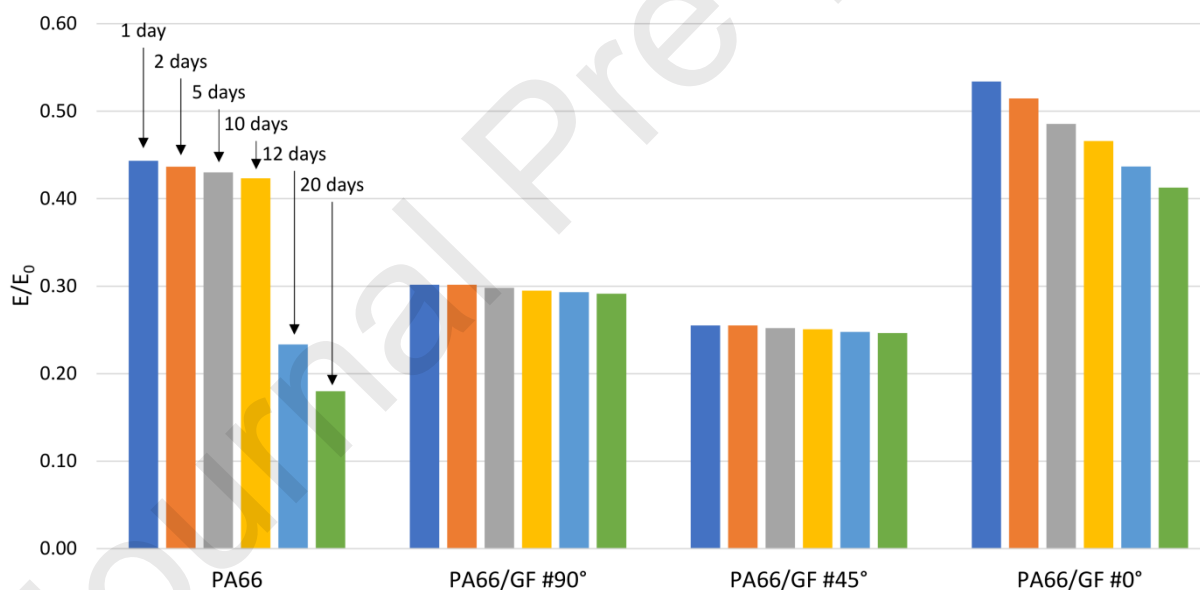


Figure 10. Stiffness degradation for unreinforced and short glass fiber reinforced PA66 samples aged in glycol for 1 day, 2 days, 5 days, 10 days, 12 days, and 20 days.

One can notice that the absorption of the glycol brings about a significant decrease of mechanical properties in terms of strength (Figure 9). This degradation occurs together with the swelling of the samples cross-section (Figure 8). In fact, once the PA66 samples are immersed in glycol at 130 °C, regardless of the aging duration, hydrogen bonds are formed between the amide groups of the polymer and the hydroxyl roots of the alcohol function in the glycol. This effect can be described in three stages; the first stage occurs up to 2 days of

aging, in which the mechanical response shows a deformability increase accompanied with a significant drop of the stress at failure. This phenomenon is due to the plasticization effect occurring with the glass transition decrease and leading hence the polymer to exhibit a rubbery behavior at room temperature. Indeed, the increase of the deformability is also partially induced by the increase of the distance between macromolecular chains and the subsequent free volume allowing an early glass transition temperature. Indeed, under the aging conditions, the intrusion of the glycol molecules creates more distance between the macromolecular chains of the polyamide and increases their mobility while creating more “free space” in the material. In addition, as reported in [6], [7], it is established that the glycol penetration in the material results in a drop of crystallinity rate by breakage of the macromolecular chains of the polymer [6], [7]. Furthermore, since the polyamide has a semi-crystalline microstructure, the crystalline phase decreases while the amorphous phase increases allowing the material to absorb more glycol as noticed through the mass variation (Figure 6). This aspect can be explained by analogy with the water absorption as described by Obeid et al. [25]. Indeed, the authors suggested the presence of three types of water interactions with PA6 molecules: the first type forms of a single hydrogen bond, whereas the second type forms two hydrogen bonds. The latter has one free hydrogen molecule that represents the molecular linking site for the third type of water. This last type occurs in form of chains that evolves into clusters of water molecules creating a water concentration gradient within the material and resulting into the swelling phenomenon that is observed since the first day of aging. In that sense, Puffr and Sebenda [26] have made the same observations as the 3 types detailed above (see Figure 11). They suggested a strongly linked water molecule forming two hydrogen bonds with two polyamide molecular chains, and a weakly linked water molecule forming one hydrogen bond. It is worth mentioning that the temperature and pressure promote the aforementioned absorption mechanisms.

The second stage of glycol absorption appears for the aging duration between 2 days and 10 days, in which a relative material deformability reduction is observed while the stress at failure remains in the same range. This loss of this deformability is attributed to the fact that the material undergoes a recrystallization phenomenon similar to the water effect [7] under the aging conditions effect in terms of pressure and temperature. The macromolecular chains in the amorphous phase are being restructured and transform into a crystalline phase. In this second stage, it is worth noticing that the mass variation due to the absorption of the glycol remains roughly constant. The polyamide hence reaches its absorption limit of glycol (saturation).

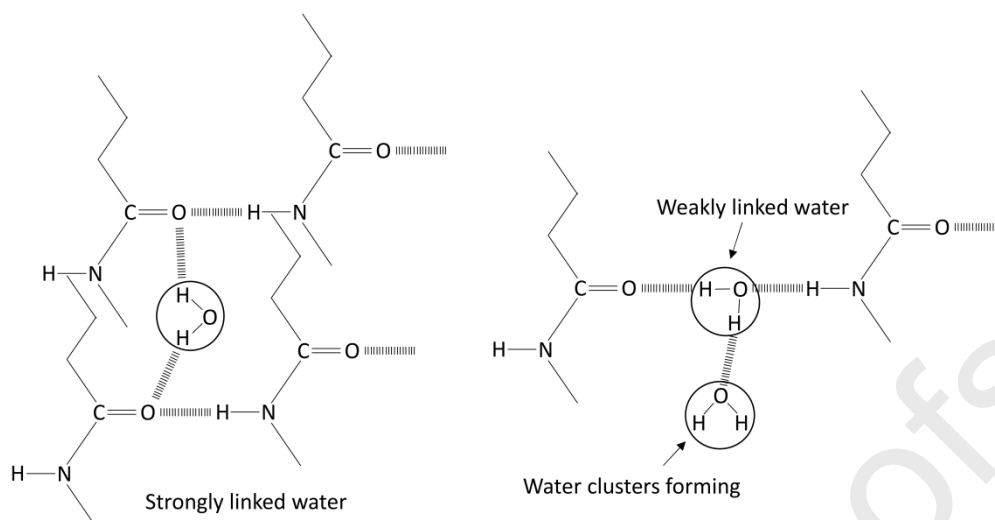


Figure 11. Types of water interacting with the polyamide [26]. It is claimed that the water contained in the polyamide is linked in 3 different ways; Strongly linked water: forming two hydrogen bonds with two polyamide molecular chains, weakly linked water: forming one hydrogen bond with two polyamide molecular chains, and water clusters: water molecules forming chains that evolve into clusters.

The third stage occurs above 12 days of aging, in which a significant embrittlement and a loss of the mechanical properties of the material are observed (Figure 9). Indeed, the aging conditions at 130 °C during 12 or 20 days in glycol cause the accumulation of macroscopic cracks which lead to a drastic material degradation as shown in Figure 7. The initiated cracks represent empty spaces that are subsequently filled with glycol hence leading to the noticed increase of the mass variation above 12 days of aging. As mentioned above, the material undergoes a recrystallization in which the amorphous phase is reorganized as a crystalline phase. The polyamide exhibits then a relative brittle mechanical response. Knowing that the crystalline phase does not absorb nor interact with the glycol as much as the amorphous phase, more glycol is kept inside the material, increasing the size of the clusters and creating accordingly higher hydrostatic pressure between the well-structured crystallites. This phenomenon results hence in the initiation and accumulation of macro-cracks leading to the material degradation.

In a related note regarding the short glass-fiber reinforced polyamide, the glycol absorption is not as advanced as the non-reinforced polyamide. It has been established that the short glass fibers are not as affected by the glycol or the temperature since they are protected and covered by the matrix and the interface [7]. However, the presence of the reinforcement reduces the absorption capacity of the glycol by the material compared to the unreinforced polyamide (Figure 6). In addition, the fiber orientation does not have a noticeable effect of the glycol absorption by the material since all the microstructure have the same reinforcement content.

Even though the glycol absorption by the composite material is restricted to the matrix, the absorption scenario is limited to the first and second stages described previously for the polyamide matrix. The first stage exhibits a plasticization effect up to 2 days of glycol aging, leading to an increase in ductility and a significant drop in the stress at failure. The second stage takes place above 2 days of aging; where the ductility is decreasing as the aging duration is higher, and the stress at failure remains roughly in the same range. Unlike the polyamide matrix, the third stage in which the material undergoes a significant embrittlement is not noticed for the reinforced polyamide composites; no macro-cracks have been observed on the surface of the samples, and no embrittlement has been noted above 12 days of aging. The absence of the third stage can be explained by the presence of glass fiber reinforcement. As described for the polyamide, the brittle failure of the polyamide is due to the hydrostatic pressure caused by the glycol clusters imprisoned in the material as these clusters increase in size. This hydrostatic pressure causes not only the matrix degradation but also the matrix/fiber interface debonding for the composites. Knowing that the interaction between the glycol and the polyamide is occurring in a molecular scale, the damaged interfaces represent vast drains for the glycol clusters from which the excess of glycol is expunged and evacuated from the material, limiting the damage of the matrix, and preventing the samples from a significant swelling.

4.3. Damage mechanisms observation using Scanning Electron Microscopy and X-ray microtomography

To identify the damage mechanisms occurring after monotonic tensile loading, post-mortem observations in the shell layer have been conducted using SEM on PA66/GF at 90° samples aged in glycol at different aging durations. The observed specimens have been extracted close to the fracture zone.

In order to have a general view of the damage phenomenon, observations with different magnifications have been performed. Figure 12 displays some of the magnifications used to observe the samples. The dark spots represent the damage in the material. The magnification (x100) provides a wider view of the sample. The fibers distribution is mainly observed at 90° in the shell, as expected. Although damage can be observed at this magnification, the damage mode cannot be properly identified. The x200 magnification provides a better precision, and allows a better investigation of the damage. The x400 magnification presents a focused view of the damage, enabling the determination and identification of the damage mechanisms mode. Starting from the x800 magnification, the damage detail on the surface is also apparent, such as cavities in the matrix and deformation bands close to the interface zone.

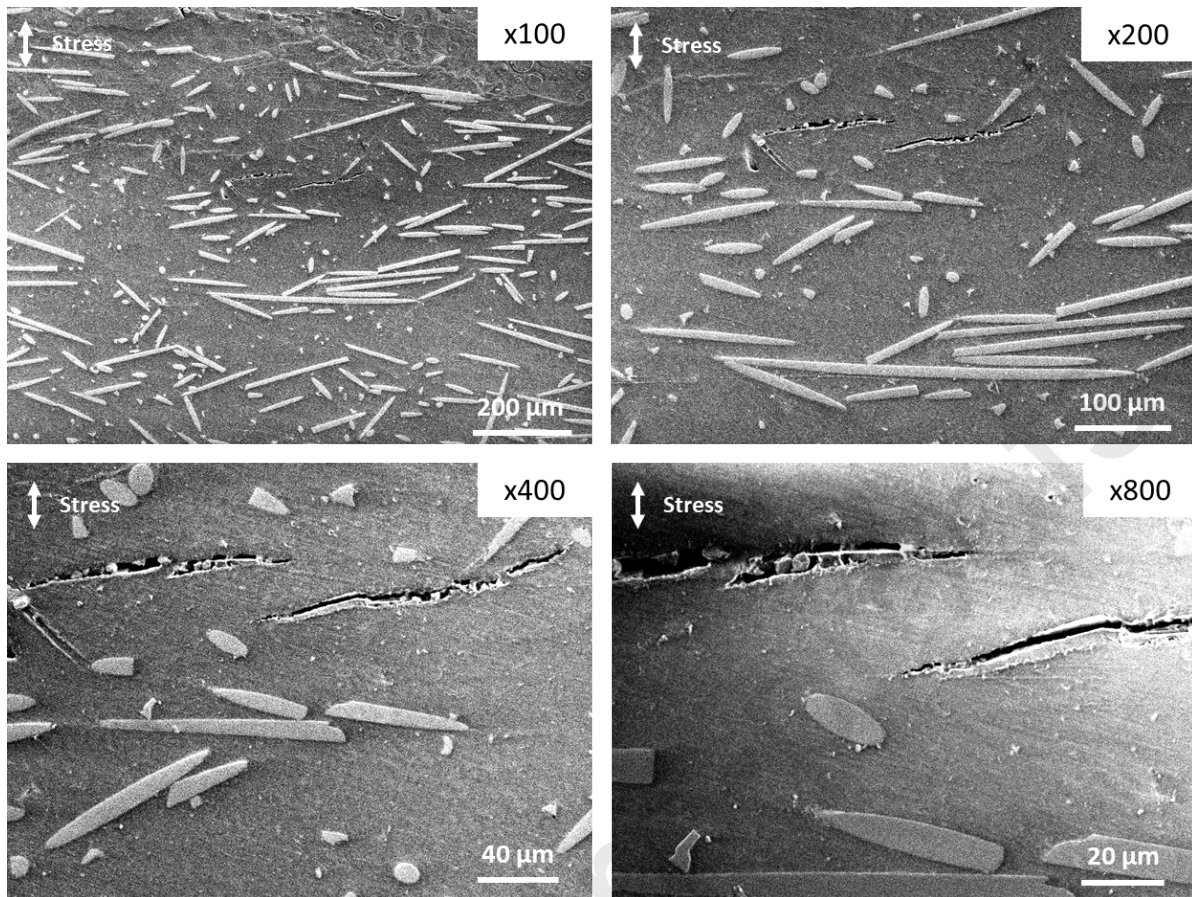


Figure 12. 10 days glycol aged PA66/GF samples at 90° SEM observations at different magnifications: x100, x200, x400, and x800. Each magnification allowing to determine the fiber orientation distribution in the material, to identify the damage location, and to define the nature of the damage mechanisms occurring.

The post-mortem observations for the different aging durations are displayed in Figure 13. For the unaged sample, the damage is barely visible at the fiber ends. It is caused by the mechanical load following the monotonic tensile tests. The matrix does not exhibit a severe damage state. For the 1day aged samples, the damage at the fibers end is more pronounced than the unaged sample, however, the damage is not widespread. For the 2 days aged sample, it is observed that the damage at the fibers ends is more pronounced than previous states. This damage is evolving into fiber/matrix debonding at a low magnitude partially in some fibers. In the 5 days aged specimen, the damage is observed at the fiber ends such as the previous specimens. The matrix/fiber debonding appears to be more extended to a longer area around the fiber, especially in the adjacent fibers. Regarding the 10 days aged sample, the damage at the fiber's ends appears to be more marked, as it extends to a more intensive fiber/matrix debonding. In addition to that, some microcracks are initiated in the matrix as well. For the 12 days aged sample, the damage at the fiber's end extends to the length of the fiber in the form of fiber/matrix debonding. The matrix exhibits also a localized damaged with the presence of cavities. One can claim that the 12 days aging duration is critical in which the matrix is significantly affected by the glycol. As for the 20 days aged sample, two observations

are presented, the observation 20D (a) displays matrix strained cupules induced by creep in which pits on the surface are forming a certain topography. The observation 20D (b) is more magnified with the purpose of displaying how the matrix is debonded around the fiber, underlining the strong fiber/matrix debonding. The damage at fibers ends and fiber/matrix debonding are observed around more fibers, but also the matrix deformed regions induced by the creep phenomenon, that appears more emphasized than the other aging durations. As expected from the monotonic tensile tests, the matrix degradation exhibits significant reduction of mechanical properties. The high level of cavities is also consistent with the evolution of the cross-section variation that is significantly higher than the other aging durations.

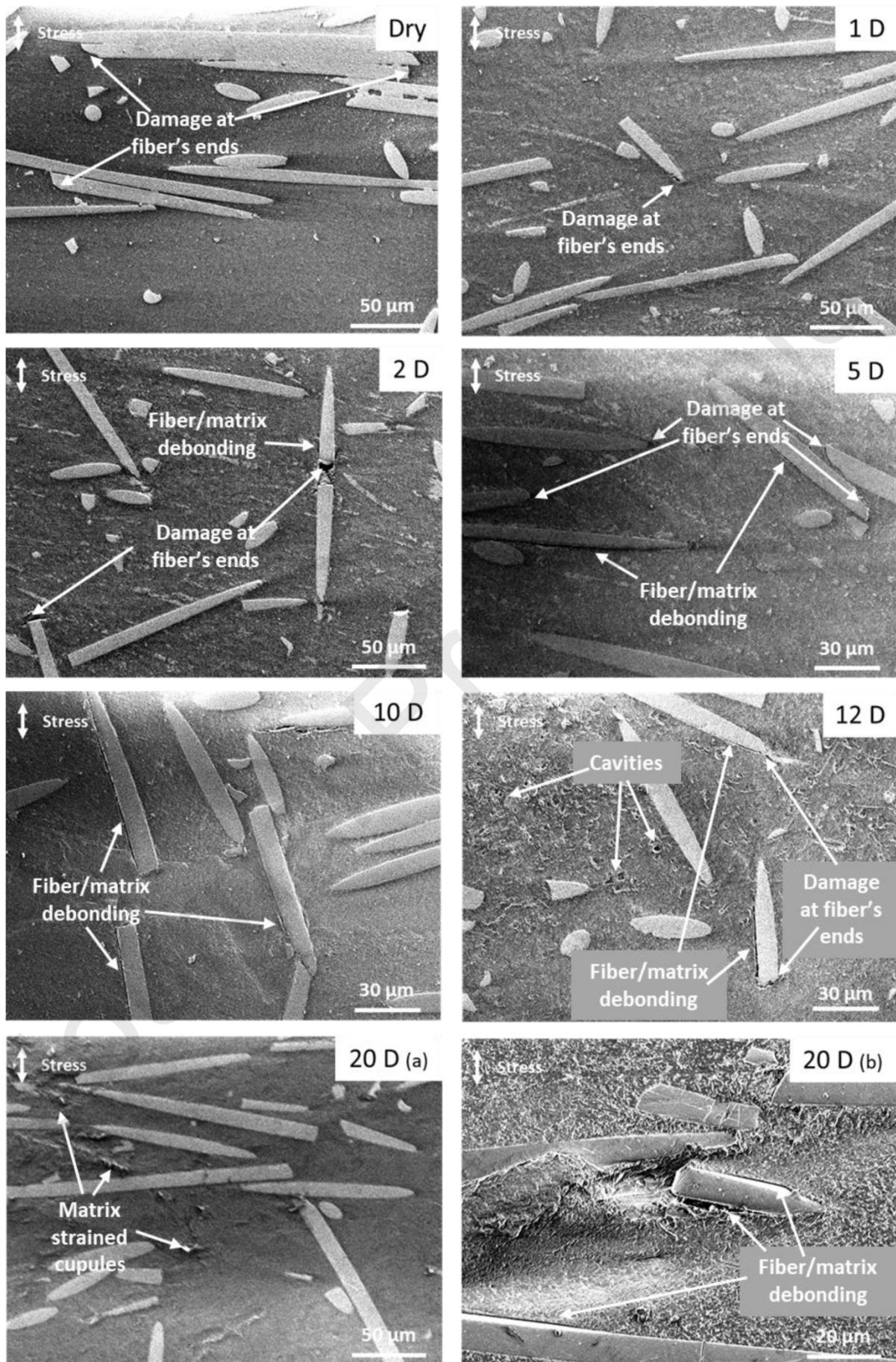


Figure 13. SEM observations for unaged (dry), 1 day, 2 days, 5 days, 10 days, 12 days and 20 days aged in glycol PA66/GF samples at 90°. The predominant damage mechanisms are damage at fibers' end, matrix/fiber debonding, and cavitation for long duration (12 and 20 days). The observed damage mechanisms are of similar nature, related to the microstructure, however, the intensity of the damage is evolving with the aging duration.

In a related note, it is possible to link the damage mechanisms occurring in glycol aged samples to the damage mechanisms related to relative humidity. Arif et al. [11] has conducted in-situ damage mechanisms investigation for PA66/GF in three relative humidity conditions (RH = 0 %, 50 %, 100 %). For all the relative humidity conditions, no damage has been noted in the initial state prior to mechanical loading. Similar damage mechanisms have been observed in all the specimens, namely: damage at fibers end, fiber/matrix debonding, matrix microcracks and fiber breakage whose accumulation leads to the macroscopic failure. The main difference consists in how microcracks evolve and to what extent. For the RH0 specimen (dry), the propagation of microcracks is rapid since the polymer exhibits a relative brittle behavior, while the propagation is slower for the other relative humidity conditions due to the relative ductile response induced by the water uptake. For the RH100 specimen, some deformation bands are more apparent due to the advanced fiber/matrix debonding. In addition, Wang et al. [27] have studied the damage mechanisms due to hygrothermal aging of novel composite material undergoing flexural loading. The latter consists of PA6 matrix containing short carbon fibers and reinforced by printed continuous glass fiber. The investigated aging durations under hygrothermal conditions are as prepared (unaged), 15, and 30 days. Regardless of the aging duration, the observed damage mechanisms are in total accordance with those observed by Arif et al. [11] and in this work for PA66/GF30. Based on the results above, in terms of damage mechanisms for both hygro and glycol aging, one can observe the same damage mechanisms that can be related to the material and its microstructure. It is worth mentioning that the relative humidity conditioning may not cause any damage nor degradation to the material while the glycol aging brings about an initial damage state before applying the mechanical loading, which explains partially brittle response of the material when tested.

Generally, crack initiation at fibers ends and matrix/fiber debonding are the main damage mechanisms observed. The matrix/fiber debonding is initiated at the adjacent fibers. One can claim that the damage is more pronounced as the aging duration increases. Cavities are observed for the higher aging durations. These cavities cause the embrittlement of the material undergoing a long aging duration. From these observations, it is possible to discriminate two types of damage mechanisms; the ones generated by the tensile loading, such as fibers breakage, damage at fiber ends and fiber/matrix debonding, and other damage mechanisms caused by the glycol absorption that mostly affect the matrix, such as the generation of cavities, bands of deformation induced by the

creep. The glycol absorption could also affect the intensity of the damage at the fibers end and the fiber/matrix interface, in a way that the matrix is more brittle and easily damaged. It would be then interesting to quantify the damage and its evolution for the different aging duration in order to properly study the glycol aging effect, that is conducted through a statistical analysis of void content in the following section, in which the voids correspond to the created damage.

4.4. Void analysis using X-Ray microtomography

As it has been observed in SEM observations, the damage increases with the aging durations. Thus, it is important to study and quantify this damage evolution. An X-ray microtomography investigation has been performed, aiming to measure the void density, the average void size, and the number of voids depending on the position through the thickness. The region used for this X-ray microtomography is the same as the one in Figure 1.a. It has been chosen for the tested specimens at different loading levels in order to prevent the stress concentration effect in the specimen (Saint-Venant principle) as well as the edge effects. The observed area is representative for the diffuse damage. The resolved measurement is performed using a voxel size of $2.04\ \mu\text{m}$. The reconstruction is made for a volume of 3 mm by 3 mm with 3 mm initial thickness. The average number of slices is 1462 slice per acquisition. Depending on the swelling, between 13 and 16 slices are analyzed using *ImageJ*[®] software. The slices are transformed into 8-bits grey scales images before the thresholding procedure for each slice, as described in Figure 14 In this figure, the voids are represented by the darkest black shades that are isolated in order to be analyzed and quantified. The void fraction, number of voids and mean void size are then obtained and plotted as discretized values through the thickness of the samples.

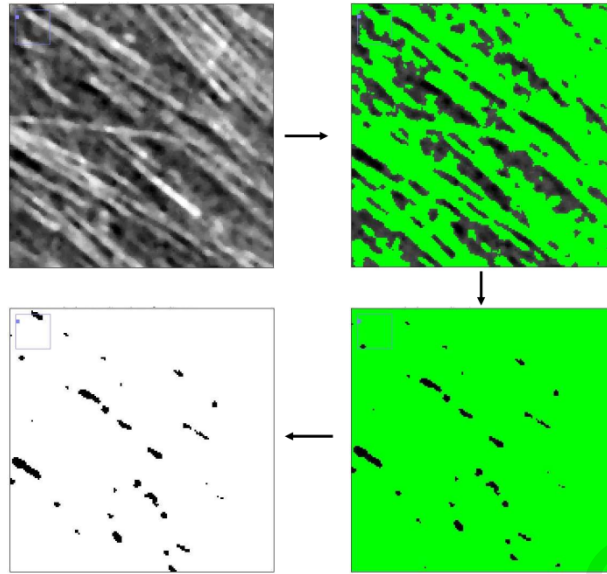


Figure 14. Thresholding procedure steps followed for the quantitative and qualitative investigation of voids in the tested materials.

The investigation has been conducted through different material configurations and aging durations. Firstly, highlighting the aging duration effect of the glycol on the damage evolution for PA66/GF with 90° and 0° fibers orientations. Figure 15 displays void fraction (Figure 15.a), the mean void size (Figure 15.b), and the number of voids (Figure 15.c) for PA66/GF at 90° at different aging durations. Generally, it is observed that the void fraction increases with the increase of aging duration. It is also noted that the void distribution is more located in the core and the surface zones of the sample due to its shell-core microstructure. The same observations are made for the mean void size and the number of voids as it increases with aging duration, except for the 5 days aged sample that shows a slight decrease in the mean void size, compensated with a relatively higher number of voids. The same phenomenon is observed for the PA66/GF at 0° (Figure 16). This can be explained by the “free volume” and the distance created between the macromolecular chains, as they are reorganized by the glycol absorption, creating a high number of voids with a low void mean size, as the latter gets increased for long aging duration.

The investigation is then carried out on the same aging durations for different materials. It clearly shows the effect of the microstructure and how the glycol aging affects the damage occurring. Figure 17 displays the void fraction (Figure 17.a), the mean void size (Figure 17.b) and the number of voids (Figure 17.c) depending on the position in the thickness. For the PA66/GF at 0° and 90° , it is noted that the voids are mostly located on the core and the surface of the sample. However, for the PA66/GF at 45° , the void at the surface is more pronounced than the core area, and is uniformly distributed in the rest of the sample. This is induced by the fibers orientation that does not emphasize the shell-core microstructure of the material in which the fibers at the edge on both the shell

and the core of the material allows an easier absorption and desorption of the glycol. In a related note, the PA66 sample shows a localization of the voids at its surface only, with a lowest localization in the middle of the sample.

430 This is due to the absence of the shell-core structure since there are no fibers. This void distribution can be explained by the surface state of the sample, as illustrated by the Figure 7.c, in which cracks are apparent on the surface. In addition, the glycol molecule diffusion is not homogenous through the thickness due to the shell-core microstructure gradient highlighted in the work of Laügt [28].

Another observation has been performed for a PA66/GF sample at 90° aged for 20 days in glycol. Figure 435 18 displays the void fraction (Figure 18.a), the average void size (Figure 18.b) and the number of voids (Figure 18.c) depending on the position in the thickness. This time, the goal is to study the damage evolution on the same sample in different areas of interest. The first area is located next to the rupture area, while the second observed region is far away from the rupture zone in the gage part. The main observations not only show the void localization in the core and the surface of the material due to the shell-core microstructure, but also imply higher damage level 440 next to the rupture zone.

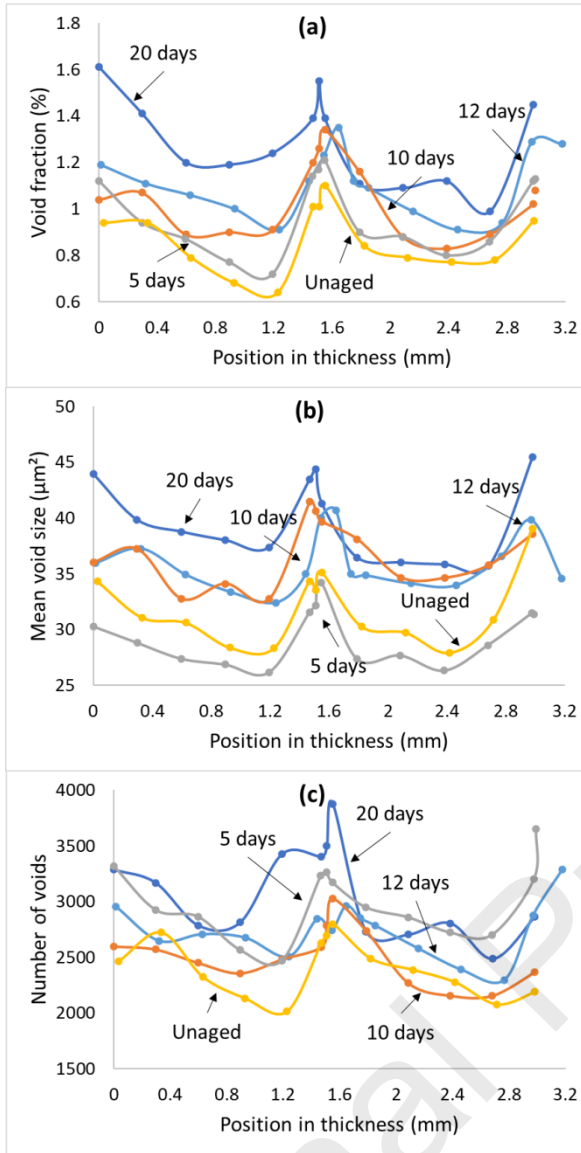


Figure 15. X-ray micro-tomography void investigation through the thickness of PA66/GF samples with fibers transversally-oriented. The investigation is conducted for both unaged, and aged samples in glycol at 5 days, 10 days, 12 days and 20 days. (a) Void fraction (%). (b) Mean void size. (c) Number of voids.

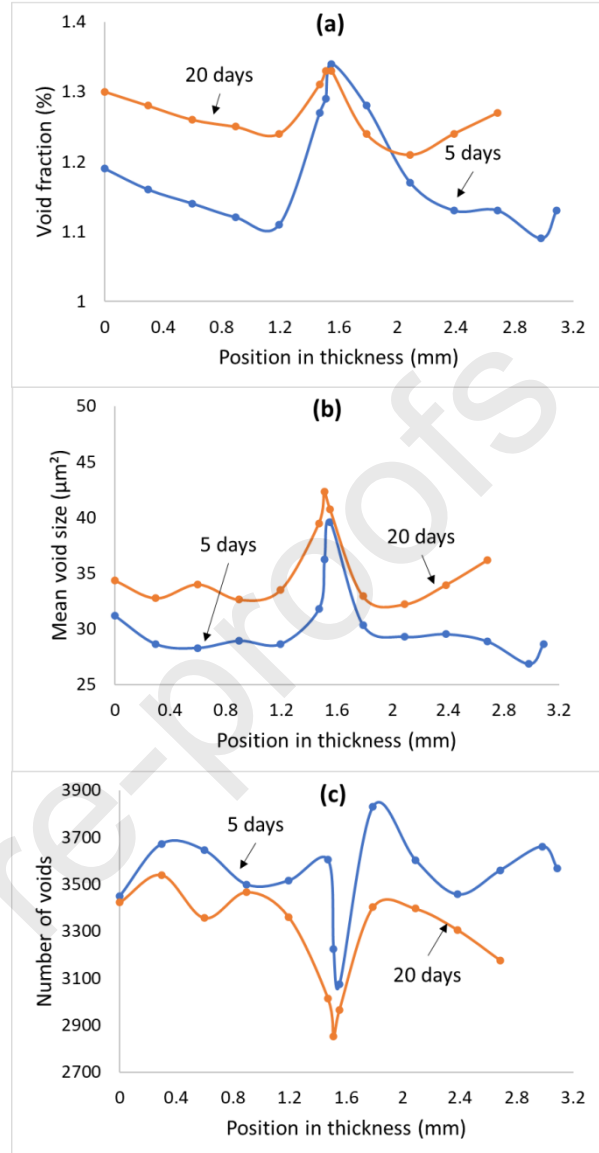


Figure 16. X-ray micro-tomography void investigation through the thickness for PA66/GF samples with fibers longitudinally-oriented. The investigation is conducted for aged samples in glycol at 5 days and 20 days. (a) Void fraction (%). (b) Mean void size. (c) Number of voids.

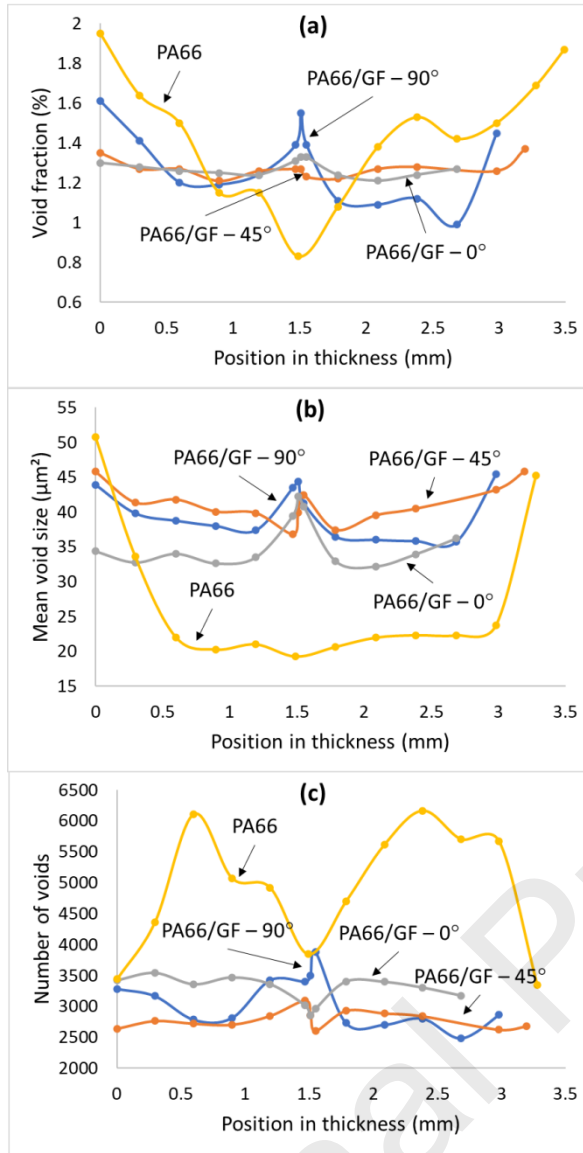


Figure 17. X-ray micro-tomography void investigation through the thickness for PA66 and PA66/GF samples with 0°, 45° and 90° oriented fibers, samples aged in glycol for 20 days. a. Void fraction (%). b. Void mean size. c. Number of voids.

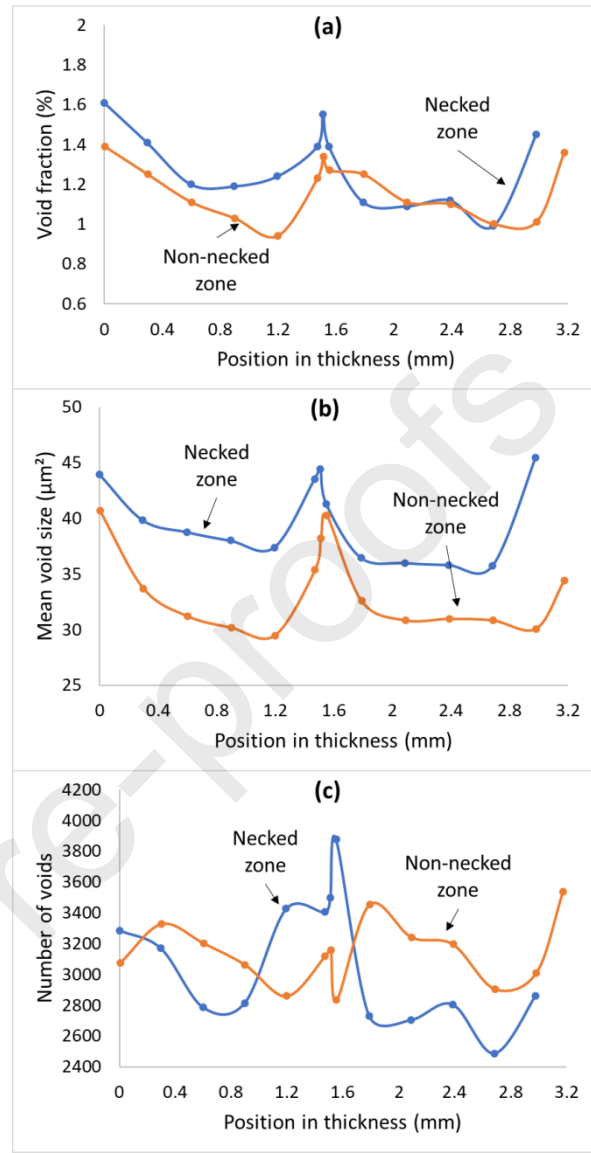


Figure 18. X-ray micro-tomography void investigation through the thickness for PA66/GF a sample with fibers transversally-oriented aged for 20 days, in the necked zone next to the rupture area and in the non-necked zone far from the rupture area. a. Void fraction (%). b. Void mean size. c. Number of voids.

5. Conclusions and further work

In this work, an experimental investigation has been conducted to study the effect of ethylene glycol aging on the PA66 and the short glass fiber reinforced PA66 overall tensile responses, and specially the impact on the damage mechanisms in terms of initiation and accumulation. Different aging durations have been taken into account to analyze the glycol aging impact on a wide range of durations, namely: 1 to 20 days. Several aspects of the aging effect have been investigated, such as the visual aspect of the sample surfaces, the mass and cross-section

variation due to the absorption of the glycol, the mechanical response under monotonic tensile tests, and damage mechanisms investigation. The latter has been conducted qualitatively and quantitatively using SEM and X-ray microtomography analyses. The main experimental findings that can be retained from this work are summarized as follows:

- The glycol absorption is more important for the non-reinforced PA66 samples than the reinforced PA66 due to the absence of glass fiber reinforcement. However, the short glass fibers orientation slightly affects the glycol concentration in the material in a way that the glycol desorption in the PA66/GF at 90° and 45° are higher than the one noticed for the PA66/GF at 0°. The fiber orientation does not seem to be affecting the glycol absorption.
- The stiffness and deformability of the tested materials are significantly affected by the glycol absorption. The stress at failure is decreased by almost half, whereas the strain at failure increases up to 4 times exhibiting a rubbery behavior compared to the unaged configuration of materials. The PA66 samples is drastically damaged after long aging durations compared to the reinforced samples, displaying 80% stiffness degradation versus 60-75% for the composites. The damage caused by the glycol aging above 12 days can be noticed visually through cracks on the surface of the samples. The PA66/GF samples, however, exhibit a stiffer behavior for the same aging duration, whereas the PA66/GF at 0° is less affected than the other fibers orientations.
- The main damage mechanisms observed for the glycol aging are: 1) Damage at fibers end, 2) Matrix/fiber debonding, 3) matrix cavitation. The latter is barely noticeable for the short aging duration (1 and 2 days). However, the level of the damage mechanisms depends on the aging durations, which lead to the damage accumulation when increasing. Compared to the damage mechanisms investigated under water uptake (relative humidity), one can claim that the specific damage mechanisms observed under glycol aging are similar and related to the microstructure of the material. Moreover, the damage is initiated at fiber ends and it propagates along the reinforcement interface.
- The shell-core microstructure plays an important role in the damage distribution through the thickness of the material. Indeed, the damage is mostly located at the core of the material, as well as the surface (skin) that is in direct contact with the glycol. However, the microstructure does not seem to have a significant effect on the damage distribution for the PA66/GF at 45°. For the non-reinforced matrix samples on the other hand, and due to the absence of the fibers, the damage is mostly localized on the surface and gradually decreasing towards the center of the material.

The present work has been mainly focused on the glycol aging effect on the PA66/GF behavior, with a main focus on the damage mechanisms. However, further work is currently conducted to identify deeply the damage chronology through in-situ tests, either via X-ray microtomography or SEM. It will be crucial in order to distinguish the initial damage induced by glycol aging, and the subsequent one caused by mechanical loading. In a related note, a similar experimental campaign regarding coolant aging effect on the PA66/GF behavior will also be conducted with a main focus on the damage mechanisms investigation. In this framework, the work presented in this paper will be the foundation of the coolant aging effect on the damage mechanisms investigation, in which both water and glycol aging interactions with the material will be combined. Therefore, it will be possible to determine whether the water and glycol effects on the PA66/GF are antagonist or in synergy and to what extent.

Acknowledgement

This work has been conducted in the framework of the THERMOFIP project (FUI project), led by DOMO Chemicals. The authors gratefully acknowledge DOMO Chemicals for supporting this work, providing the test material and glycol, along with the shared knowledge and practical tips that allowed improving the glycol aging setup and ensuring safety measures, as well as the partners of the THERMOFIP project for the fruitful discussions and suggestions about the conducted work. The authors also wish to warmly thank Dr. Laurent Peltier for his support in the various experimental testing aspects of the presented work, as well as Djamel Meziani regarding the samples water-jet machining, Olivier Perroud in the X-ray microtomography part, and Marc Warry for his support for the SEM observations.

References

- [1] A. Benaarbia, A. Chrysochoos, and G. Robert, "Influence of relative humidity and loading frequency on the PA6.6 cyclic thermomechanical behavior: Part I. mechanical and thermal aspects," *Polym. Test.*, vol. 40, pp. 290–298, 2014.
- [2] A. Benaarbia, A. Chrysochoos, and G. Robert, "Influence of relative humidity and loading frequency on the PA6.6 thermomechanical cyclic behavior: Part II. Energy aspects," *Polym. Test.*, vol. 41, pp. 92–98, 2015.
- [3] A. Benaarbia, A. Chrysochoos, and G. Robert, "Thermomechanical behavior of PA6.6 composites subjected to low cycle fatigue," *Compos. Part B Eng.*, vol. 76, pp. 52–64, 2015.
- [4] V. Fabre, G. Quandalle, N. Billon, and S. Cantournet, "Time-Temperature-Water content equivalence on dynamic mechanical response of polyamide 6,6," *Polymer (Guildf)*, vol. 137, pp. 22–29, 2018.
- [5] H. Obeid, "Durabilité de composites à matrice thermoplastique sous chargement hygro-mécanique : étude multi-physique et multi-échelle des relations microstructure-propriétés-états mécaniques," Université de Nantes, 2016.
- [6] B. Ledieu, "Vieillissement en milieu eau/glycol du polyamide 66 renforcé fibres de verre courtes pour l'application boîte à eau de radiateur de refroidissement moteur," Arts et Métiers ParisTech, 2010.
- [7] I. Pires, "Vieillissement dans l'antigel de matériaux composites polyamide-6,6 renforcé par des fibres de verre courtes," Université de Montpellier II, 2000.

- 515 [8] M. F. Arif, N. Saintier, F. Meraghni, J. Fitoussi, Y. Chemisky, and G. Robert, "Composites : Part B Multiscale fatigue damage characterization in short glass fiber reinforced," *Compos. PART B*, vol. 61, pp. 55–65, 2014.
- [9] E. Baquet, "Modélisation thermomécanique visco-hyperélastique du comportement d'un polymère semi-cristallin : application au cas d'une matrice polyamide 6.6," Université PSL, Mines ParisTech, 2011.
- 520 [10] A. Benaarbia, "Analyse énergétique du comportement thermomécanique du PA6.6 chargé de fibres de verre," Université de Montpellier II, 2014.
- [11] M. F. Arif, F. Meraghni, Y. Chemisky, N. Despringre, and G. Robert, "Composites : Part B In situ damage mechanisms investigation of PA66 / GF30 composite : Effect of relative humidity," *Compos. PART B*, vol. 58, pp. 487–495, 2014.
- 525 [12] H. Rolland, N. Saintier, and G. Robert, "Damage mechanisms in short glass fibre reinforced thermoplastic during in situ microtomography tensile tests," *Compos. Part B*, vol. 90, pp. 365–377, 2016.
- [13] S. Eckel, F. Meraghni, P. Pomarède, and N. F. Declercq, "Investigation of Damage in Composites Using Nondestructive Nonlinear Acoustic Spectroscopy," *Exp. Mech.*, vol. 57, no. 2, pp. 207–217, 2017.
- 530 [14] N. Miqoi *et al.*, "Detection and evaluation of barely visible impact damage in woven glass fabric reinforced polyamide 6.6/6 composite using ultrasonic imaging, X-ray tomography and optical profilometry," *Int. J. Damage Mech.*, vol. 30, no. 3, pp. 323–348, 2021.
- [15] P. Marguères and F. Meraghni, "Damage induced anisotropy and stiffness reduction evaluation in composite materials using ultrasonic wave transmission," *Compos. Part A Appl. Sci. Manuf.*, vol. 45, pp. 134–144, 2013.
- 535 [16] N. Sato, T. Kurauchi, S. Sato, and O. Kamigaito, "Microfailure behaviour of randomly dispersed short fibre reinforced thermoplastic composites obtained by direct SEM observation.," *J Mater Sci*, vol. 26, 1991.
- [17] J. Horst and J. Spoormaker, "Fatigue fracture mechanisms and fractography of short-glassfibre-reinforced polyamide 6.," *J Mater Sci*, 1997.
- 540 [18] J. Horst, N. Salienko, and J. Spoormaker, "Fibre-matrix debonding stress analysis for short fibre-reinforced materials with matrix plasticity, finite element modelling and experimental verification.," *Compos Part A*, 1998.
- [19] H. Rolland, N. Saintier, P. Wilson, J. Merzeau, and G. Robert, "In situ X-ray tomography investigation on damage mechanisms in short glass fibre reinforced thermoplastics : Effects of fibre orientation and relative humidity," *Compos. Part B*, vol. 109, pp. 170–186, 2017.
- 545 [20] M. F. Arif, "Mécanismes d'endommagement du polyamide-66 renforcé par des fibres de verre courtes, soumis à un chargement monotone et en fatigue : Influence de l'humidité relative et de la microstructure induite par le moulage par injection Muhamad Fatikul Arif To," Arts et Métiers Paristech, 2014.
- 550 [21] B. Klimkeit, "Etude expérimentale et modélisation du comportement en fatigue multiaxiale d'un polymère renforcé pour application automobile," Ecole nationale supérieure de mécanique et d'aéronautique, 2009.
- [22] H. Rolland, "Comportement en fatigue et mécanismes d'endommagement du polyamide 6,6 renforcé de fibres courtes – Application à la fatigue sous chargement d'amplitude variable," Arts et Métiers ParisTech, 2017.
- 555 [23] Q. Chen, G. Chatzigeorgiou, G. Robert, and F. Meraghni, "Viscoelastic-viscoplastic homogenization of short glass-fiber reinforced polyamide composites (PA66/GF) with progressive interphase and matrix damage: New developments and experimental validation," *Mech. Mater.*, vol. 164, p. 104081, 2022.
- 560 [24] I. Panaitescu, T. Koch, and V.-M. Archodoulaki, "Accelerated aging of a glass fiber/polyurethane composite for automotive applications," *Polym. Test.*, vol. 74, pp. 245–256, 2019.
- [25] H. Obeid, A. Clément, S. Fréour, F. Jacquemin, and P. Casari, "On the identification of the coefficient of moisture expansion of polyamide-6: Accounting differential swelling strains and plasticization," *Mech. Mater.*, vol. 118, pp. 1–10, 2018.
- [26] R. Puffr and J. Šebenda, "On the Structure and Properties of Polyamides. XXVII. The Mechanism of

- 565 Water Sorption in Polyamides,” *J. Polym. Sci. Part C Polym. Symp.*, vol. 16, pp. 79–93, 2007.
- [27] K. Wang, Y. Chen, H. Long, M. Baghani, Y. Rao, and Y. Peng, “Hygrothermal aging effects on the mechanical properties of 3D printed composites with different stacking sequence of continuous glass fiber layers,” *Polym. Test.*, vol. 100, p. 107242, 2021.
- 570 [28] C. Laügt, “Comportement mécanique d’un polyamide 6,6 soumis à un vieillissement thermo-hydro-glycolé ; Relations microstructure-propriétés,” Université PSL, Mines ParisTech, 2022.

Declaration of interests

575 ☒ The authors declare that they have no known competing financial interests or personal relationships that could have appeared to influence the work reported in this paper.

☐ The authors declare the following financial interests/personal relationships which may be considered as potential competing interests:

580